Iron and Manganese Containing Multi-Walled Carbon Nanotubes as Electrocatalysts for the Oxygen Evolution Reaction - Unravelling Influences on Activity and Stability

Cornelia Broicher,[a] Feng Zeng,[b] Norbert Pfänder,[c] Marvin Frisch,[a] Timo Bisswanger,[d] Jörg Radnik,[e] Jörg Manfred Stockmann,[e] Stefan Palkovits,[b] Anna Katharina Beine,*[c] and Regina Palkovits[b]

Hydrogen economy is a central aspect of future energy supply, as hydrogen can be used as energy storage and fuel. In order to make water electrolysis efficient, the limiting oxygen evolution reaction (OER) needs to be optimized. Therefore, C-based composite materials containing earth-abundant Fe and Mn were synthesized, characterized and tested in the OER. For pyrolysis temperatures above 700 °C N-rich multi-walled carbon nanotubes (MWCNT) are obtained. Inside the tubes Fe_3C particles are formed, Fe and Mn oxides are incorporated in the carbon matrix and metal spinel nanoparticles cover the outer surface. The best catalyst prepared at 800 °C achieves a low overpotential of 389 mV (at 10 mA/cm^2) and high stability (22.6 h). From electrochemical measurements and characterization it can be concluded that the high activity is mainly provided by MWCNT, Fe_3C and the metal oxides in the conductive carbon matrix. The metal spinel nanoparticles in contrast protect the MWCNT from oxidation and thereby contribute to the high stability.

Introduction

Environmental pollution and a rising energy consumption of the growing world population represent major global challenges. Renewable energies such as wind, solar or water power facilitate a sustainable energy supply; however, due to their temporal and spatial intermittency, concepts for energy storage are needed.[1–3] Electrochemical water splitting to generate hydrogen as portable energy source represents one possible solution.[4–6] The reaction is limited by the high overpotential (OP) of the oxygen evolution reaction (OER) (Scheme 1).[7–9] RuO_2 and IrO_2 were the first examples for highly active electrocatalysts in the OER at high pH value.[10–12] Drawbacks of these catalysts are the high raw material price and their unsatisfying stability. An alternative are non-noble mixed metal oxides.[13–14] However, such materials often suffer from low specific surface area, porosity and electrical conductivity.[15] To enhance dispersion and electron transfer, the metal oxides were supported on conductive carriers such as graphene and carbon nanotubes (CNT).[16,17] CNT provide a good electrocatalytic performance due to their conductivity, mechanical stability, chemical resistance and high specific surface area.[18–22] The stability of a metal-free CNT catalyst is yet reported to be low as deactivation occurs in under 2 h of reaction.[21] The combination with metal oxides allows an improved activity in electrochemical reactions.[23–29] Antoni *et al.*[30] prepared Mn_xO_y nanoparticles of different oxidation state on O- and N-functionalized CNT finding the highest activity for Mn in a high oxidation state. However, the reported stability was low. Masa *et al.*[31] synthesized Mn_xO_y and Co_xO_y nanoparticles embedded

$$\text{OER: } 4\,OH^- \longrightarrow O_2 + 2\,H_2O + 4\,e^-$$
$$E_0 = 1.23\text{ V } vs.\text{ RHE}$$

Scheme 1. Conversion of hydroxide anions in the oxygen evolution reaction (OER) and the needed standard potential E_0 obtained from the Nernst equation.

[a] C. Broicher, M. Frisch
Department of Chemistry
Chemical and Materials Engineering Division
Technical University Berlin
Straße des 17. Juni 124
10623 Berlin (Germany)
[b] Dr. F. Zeng, Dr. S. Palkovits, Prof. R. Palkovits
Institute of Technical and Macromolecular Chemistry
RWTH Aachen University
Worringerweg 2
52074 Aachen (Germany)
[c] N. Pfänder, Dr. A. K. Beine
Max Planck Institute for Chemical Energy Conversion
Stiftstr. 34–36
45470 Mülheim an der Ruhr (Germany)
E-mail: katharina.beine@cec.mpg.de
[d] T. Bisswanger
2nd Institute of Physics
RWTH Aachen University
Otto-Blumenthal-Str. 18
52074 Aachen (Germany)
[e] Dr. J. Radnik, J. M. Stockmann
Bundesanstalt für Materialforschung und -prüfung (BAM)
Unter den Eichen 44–46
12203 Berlin (Germany)

Supporting information for this article is available on the WWW under https://doi.org/10.1002/cctc.202000944

This publication is part of the Young Researchers Series. More information regarding these excellent researchers can be found on the ChemCatChem homepage.

in an N-doped carbon matrix. They demonstrated that the interaction of N-doped carbon and metal oxide enhances the electrocatalytic performance. In addition, they observed a rapid degradation of the catalyst after few cycles of double-pulse chronopotentiometry. Wen *et al.*[32] and Ma *et al.*[33] reported that metal nanoparticles encapsulated in a carbon matrix possess an excellent OER activity due to electronic interaction between metal and carbon tuning the redox properties of the surrounding carbon layer. Also Fe_3C has been reported to have the ability to catalyze electrochemical reactions.[34–36] Barman *et al.*[37] report an Fe/Fe_3C encapsulated N-doped CNT catalyst with long term stability over 1000 cycles. Many studies address the synthesis and characterization of electrocatalysts composed of metal oxides, metal carbides and conductive carbon as well as their application in OER.[38–40] Some authors are able to reach high activity and outstanding stability, however, these studies often lack a detailed investigation of the exact origin of the high performance of the composite materials. Herein, we report a simple strategy to prepare a catalyst consisting of Fe, Mn and N-rich carbon. Thorough characterization elucidates the catalyst structure and composition, which is used to explain influences on the OER activity and stability in an alkaline electrolyte solution.

Results and Discussion

Characterization of the electrocatalysts

To synthesize the electrocatalysts, $MnCl_2$, $FeCl_2$, and $FeCl_3$ were used as metal precursors and ground together with dicyandiamide (DCD). The choice of metals and metal ratios is based on a previous study, whose results are briefly summarized in Figures S1 and S2 in the ESI. The mixture was pyrolyzed under nitrogen atmosphere at temperatures between 600 °C and 900 °C. After pyrolysis, the catalysts were ground and washed with NaOH and H_2O to remove excess metal salts (detailed experimental procedures can be found in the experimental section). The materials were named Fe,Mn@DCD_p-*T* and characterized by N_2-physisorption, CHN, ICP-OES, Raman spectroscopy, XPS, STEM(-EDX), and XRD. All synthesized materials are porous according to N_2-physisorption analysis (Figure S3 in the ESI). They show a type IV isotherm after IUPAC and a specific surface area of up to 136 m^2/g (Table 1). The N-content of the materials obtained from elemental analysis decreases with increasing pyrolysis temperature from 20% (600 °C) to 1.5% (900 °C). Simultaneously, the C-content of the materials increases with increasing synthesis temperature from 17% to 37%. ICP-OES analysis of the materials shows a decreasing Mn-content (19 to 11 wt%) and an increasing Fe-content (32 to 42 wt.%) with increasing pyrolysis temperature.

From Raman spectroscopy two characteristic signals for carbon based materials can be identified (Figure 1): The G-band at around 1580 cm^{-1} originates from the Raman-active E_{2g} mode of graphitic carbon, while the D-band at 1350 cm^{-1} can be referred to amorphous regimes in the carbon matrix.[41] The ratio of the intensity of D- and G-band provides information

Table 1. Physical properties of Fe,Mn@DCD_p-materials: surface area was obtained from N_2-physisorption analysis using the BET-method, atomic ratio of Fe/Mn was determined via ICP-OES, elemental analysis yielded the fractions of C, H and N, the wall thickness of the multi-walled carbon nanotubes (MWCNT) was extracted from STEM images.

Material Fe,Mn@DCDp-	S_{BET} [m^2/g]	ICP-OES [wt.%]	Elemental analysis [wt.%]	Wall thickness of MWCNT [nm]
600 °C	28	32.0% Fe, 19.3% Mn	20% N, 17% C, 1.5% H	–
700 °C	136	41.2% Fe, 19.2% Mn	6% N, 28% C, 1.6% H	49 ± 13
800 °C	124	36.0% Fe, 17.6% Mn	5% N, 29% C, 1.4% H	65 ± 22
900 °C	66	42.0% Fe, 10.5% Mn	1.5% N, 37% C, 0.5% H	102 ± 18

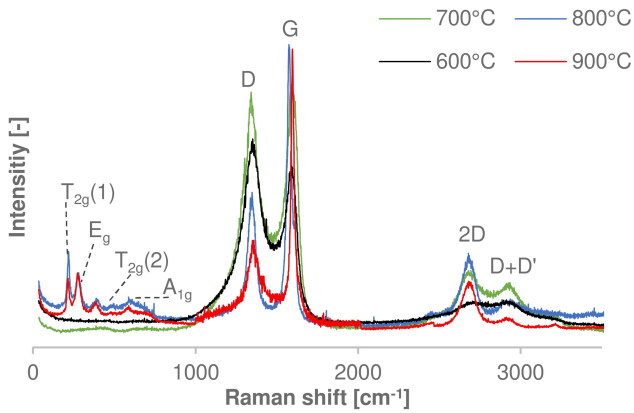

Figure 1. Raman spectroscopy of synthesized Fe,Mn@DCD_p-materials.

about the materials degree of graphitization and therefore its ability to conduct electrons. The ratio of I_D/I_G decreases for the materials with increasing pyrolysis temperature. While for a pyrolysis temperature of 600 °C an I_D/I_G ratio of 1.1 is obtained, it decreases to 0.7 for the material prepared at 900 °C proving a higher crystallinity and therefore more graphitic nature. Additionally, Raman modes at low and high wave numbers are observed.

The high frequency signals at 2650 cm^{-1} and 2900 cm^{-1} are known as the 2D and D+D′ signals corresponding to overtones.[42] The 2D signal originates from a second-order overtone of different in-plane vibrations. For samples prepared at 800 °C and 900 °C some additional signals appear at low wave numbers of 215 cm^{-1}, 277 cm^{-1}, 389 cm^{-1}, 474 cm^{-1} and 583 cm^{-1}. They can be referred to two T_{2g}, one E_g and one A_{1g} Raman mode according to literature.[43] These modes indicate the presence of Fe_3O_4 spinel on the surface of the materials.

To further elucidate the structure of the materials XPS analysis was performed. According to the XPS survey spectra of the electrocatalysts synthesized at 700 °C to 900 °C Cl, C, N, O, Mn and Fe are present on the surface (Figure S4 in the ESI). The carbon concentration decreases with increasing pyrolysis tem-

perature. Simultaneously the surface concentration of O and Fe increases. Therefore, the surface composition of the materials can be altered by tuning the pyrolysis temperature. From the element spectra (Figure S5 in the ESI), four different carbon species can be identified from the C 1s signals corresponding to sp^3- and sp^2-hybridized carbon, ether/ester- and carbonyl-groups. Two different nitrogen species corresponding to pyridinic and pyrrolic nitrogen can be identified from the N 1s spectrum. The Mn $2p_{3/2}$ and Mn $2p_{1/2}$ signals appear at a binding energy of 641.5 and 652.7 eV, respectively. Due to the low surface concentration of Mn, the signals were not fitted. Nevertheless, the binding energy indicates the presence of bi- or trivalent Mn species on the surface.[44] The Fe $2p_{3/2}$ and Fe $2p_{1/2}$ peaks show binding energies of 710.2 and 723.5 eV, respectively. The peak position, the shape of the obtained signals and the fitting indicates the presence of metal oxides, i.e. Fe_2O_3 and/or Fe_3O_4, on the surface.[45,46]

STEM analysis of the synthesized materials reveals the formation of an unstructured carbon at low pyrolysis temperature of 600 °C (Figure 2a and b). The highest I_D/I_G value of 1.1 obtained from Raman spectroscopy for Fe,Mn@DCD_p-600 °C suggests the formation of amorphous carbon (Figure S6 in the ESI). Additionally, XRD of the sample reveals no distinct peaks due to the high signal-to-noise ratio typically observed for amorphous carbon (Figure S7 in the ESI). For an increased pyrolysis temperature the formation of CNT is observed (Figure 2 c-h). These tubes are multi-walled (MWCNT) and the wall-thickness increases with increasing pyrolysis temperature to maximally 102 nm (Table 1). Small particles cover the outer surface of the MWCNT and the formation of some bigger metal nanoparticles inside the tubes is observable. STEM-EDX analysis of the materials reveals that the tubes are composed of carbon (Figures S8 to S10 in the ESI). Mn, Fe and O cover the outer surface of the MWCNT suggesting the formation of oxidic metal species. The nanoparticles inside the tubes are solely composed of Fe. Stirring of Fe,Mn@DCD_p-800 °C in 1 M H_2SO_4 for 24 h leads to the complete removal of the outer metal particles (Figure 2i and j). The resulting material is named Fe,Mn@DCD_p-800 °C-H_2SO_4. Still, Mn, Fe and O are distributed over the whole MWCNT according to STEM-EDX, so that an incorporation of metal oxides into the carbon matrix of the MWCNT is most likely (Figure S11 in the ESI).

To clearly identify the formed metal species inside and outside of the MWCNT, the materials synthesized at 700 °C to 900 °C were analyzed by XRD (Figure 3). The broadened diffraction peaks at 2θ values of 25.8° and 43.1° can be attributed to graphitic MWCNT.[47] Also Fe_3O_4 (30.0° (220), 35.0° (311), 46.0° (400), 54.0° (422), 56.0° (511), 64.0° (440)) (JCPDS no. 74-0748)[45] as well as Mn_3O_4 spinels can be identified (18.0° (101), 32.5° (103), 37.4° (211), 52.5° (105)) (JCPDS no. 24-0734).[42,48] The reflex at 44.7° additionally indicates the presence of Fe^0 (JCPDS no. 87-0722).[32] When taking a closer look into the region of 39° to 50° for materials synthesized at 700 °C and 800 °C, many small diffraction signals are visible. These signals indicate the presence of Fe_3C (39.5° (002), 40.5° (201), 42.5° (211), 43.5° (102), 44.4° (220), 48.5° (131), 49.0° (221)) (JCPDS no. 65-2411).[49] It is literature known that Fe_3C undergoes decomposition to Fe^0 and graphitic carbon at elevated temperatures, explaining why Fe_3C was not found for materials synthesized at 900 °C.[50] For Fe,Mn@DCD_p-800 °C-H_2SO_4 graphite (27.3°) (JCPDS no. 41-1487), Fe_3C (43.0° (102), 44.7° (220), 48.6° (131), 49.2° (221)), reduced Fe^0 (45.0°) as well as Fe_3O_4 (45.2° (400)) and Mn_3O_4 (37.6° (211), 52.8° (105)) are observed in the XRD spectrum (Figure S12 in the ESI). The analysis clearly proves that metal oxides are not only formed on the outer surface of the tubes but are also incorporated into the carbon matrix.

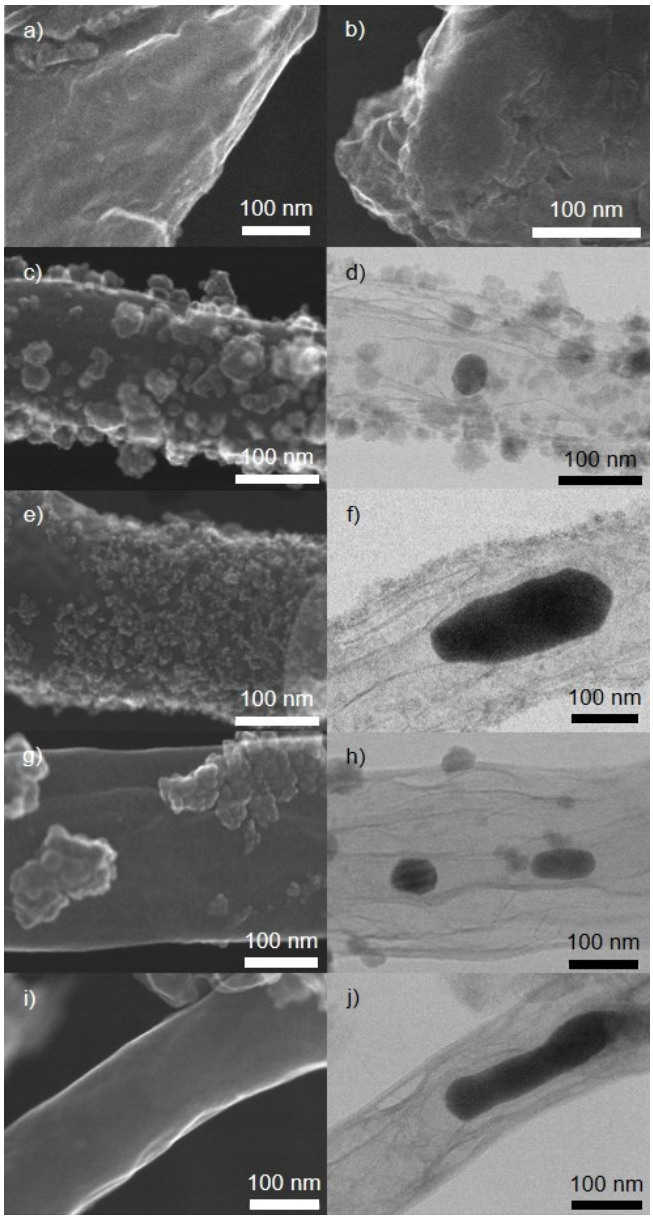

Figure 2. Secondary electron (a, b, c, e, g, i) and bright field (d, f, h, j) STEM images of prepared materials: a–b) Fe/Mn@DCD_p-600 °C, c–d) Fe/Mn@DCD_p-700 °C, e–f) Fe/Mn@DCD_p-800 °C, g–h) Fe/Mn@DCD_p-900 °C, i-j) Fe/Mn@DCD_p-800 °C-H_2SO_4.

For Fe,Mn@DCD_p-materials prepared at temperatures of 700 °C or above N-rich MWCNT are formed. They are composed of C, N and metal oxides. Inside the MWCNT, Fe_3C is formed,

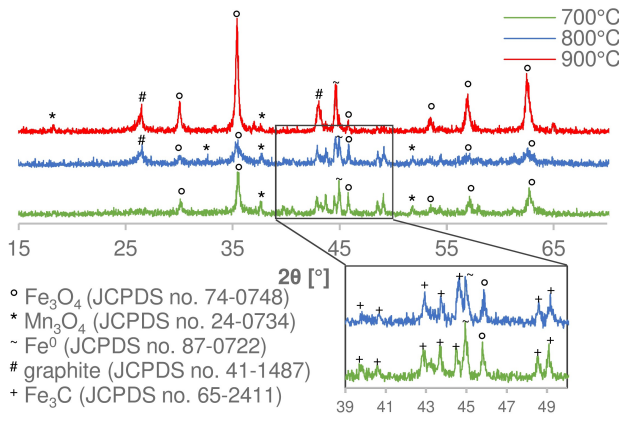

Figure 3. XRD diffraction pattern of synthesized Fe,Mn@DCD$_p$-materials prepared at 700 °C–900 °C.

which decomposes to Fe^0 at elevated temperature. The outer surface of the MWCNT is additionally decorated with Mn_3O_4 and Fe_3O_4 particles (Scheme 2 and Figure S13 in the ESI).

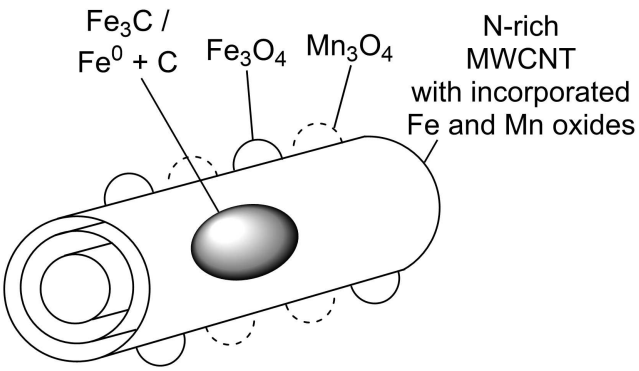

Scheme 2. Schematic illustration of the structure of the Fe,Mn@DCD$_p$-materials synthesized at 700 °C – 900 °C.

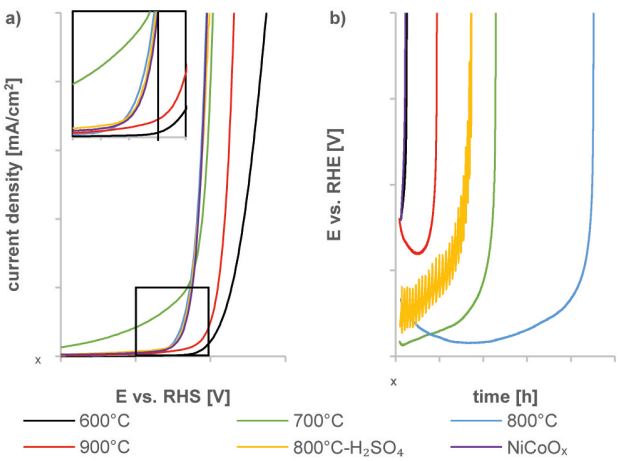

Figure 4. Comparison of electrochemical a) activity at 10 mA/cm^2 and b) stability for synthesized Fe,Mn@DCD$_p$-materials and commercial $NiCoO_x$.

Electrochemical performance of Fe,Mn@DCD$_p$-materials

The electrochemical OER activity of the prepared Fe,Mn@DCD$_p$-materials and a commercial $NiCoO_x$-catalyst was evaluated by linear sweep voltammetry (LSV) in 1 M KOH. The working electrode was a rotating disc electrode (RDE) coated with the catalyst and operated at 1600 rpm. The LSV results are depicted in Figure 4a. With an increasing synthesis temperature, the OP decreases to a minimum of 389 mV at a current density of 10 mA/cm^2 for the material prepared at 800 °C. This is comparable to the performance of $NiCoO_x$, reaching an OP of 390 mV. In addition, the H_2SO_4 treated material without spinel particles on the outer surface of the MWCNT reaches a low OP of 397 mV as well. For a further increasing pyrolysis temperature, the OP increases again. The poor performance of the material prepared at 600 °C is attributed to the absence of MWCNT and therefore to a low conductivity. With increasing pyrolysis temperature additionally, the formation of Fe_3C is facilitated. At further increased pyrolysis temperatures, anyhow, Fe_3C is decomposed to Fe^0 and graphitic carbon resulting in a decreased OER activity. The presence of the Mn and Fe spinel particles on the outer surface of the MWCNT in contrast do not have a major influence on the OER activity, as Fe,Mn@DCD$_p$-800 °C and Fe,Mn@DCD$_p$-800 °C-H_2SO_4 show a comparable performance. Fe and Mn oxides are anyhow known to be active compounds for the OER, so their role cannot be neglected.[51,52] The STEM-EDX and XRD analysis of the samples confirmed that the Fe and Mn oxides are not only present on the catalyst surface but also incorporated in the carbon matrix. Therefore, metal oxides as well as MWCNT are identified to be active species and responsible for a good activity. Additionally, an increased activity is found for materials possessing Fe_3C instead of Fe^0 particles inside the tubes, so that Fe_3C is considered as active species as well. It can on the one hand contribute to the conductivity of the electrode material and on the other hand function as adsorption site for the substrate OH^-. Even though the particles are located inside the tubes, they can be accessed by the substrate as the tubes are open at one end as seen in STEM (Figure S14 in the ESI). As temperature controls the formation of Fe_3C and MWCNT, it strongly influences the electrochemical activity of the catalysts.

For a deeper understanding of the behavior of the composite materials, electrochemical impedance spectroscopy (EIS) was carried out as shown in Figure 5a. The impedance spectra consist of a complete semicircle for all materials, which can be simulated using a Randles-circuit. In accordance with the catalytic performance, Fe,Mn@DCD$_p$-800 °C and Fe,Mn@DCD$_p$-800 °C-H_2SO_4 exhibit the lowest charge transfer resistance r_{CT} of 45 Ω and 31 Ω, respectively. The lower charge transfer resistance after the etching of the MWCNT surface using H_2SO_4 can be referred to the removal of weakly conductive metal oxide species. We further calculated the roughness factor r_F, from which the electrochemical surface area *ECSA* is derived according to equations S1 and S2 (see ESI). For the calculation of r_F the double layer capacitance c_{DL} of the composite materials is needed, which can be extracted from CV curves (1.0 to 1.1 V *vs.* RHE) at different scan rates (Figure 5b).

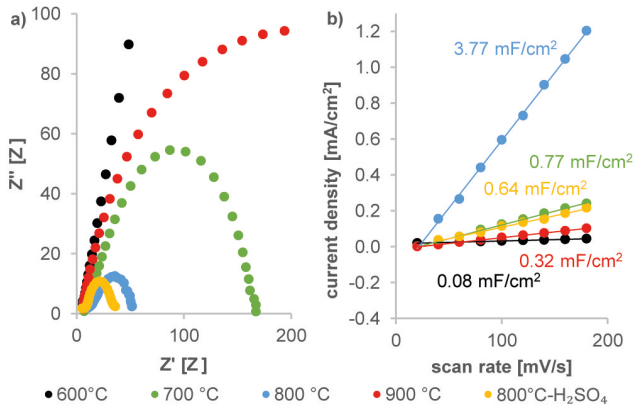

Figure 5. a) Electrochemical impedance spectroscopy (EIS) and b) double layer capacitance c_{DL} measurements for synthesized Fe,Mn@DCD$_p$-materials.

The obtained c_{DL} values vary between 0.08 and 3.8 mF/cm^2, where the highest c_{DL} value is obtained for Fe,Mn@DCD$_p$-800 °C. r_F was then used to normalize the activity and derive an intrinsic catalyst activity J_{int} (Table 2). The calculation of J_{int} is shown in equation S3 in the ESI. Fe,Mn@DCD$_p$-800 °C exhibits the highest *ECSA* (13.2 cm^2), the highest J_{int} of 0.87 mA/cm^2 is obtained for Fe,Mn@DCD$_p$-700 °C. From the data, it becomes clear that the specific surface area has no influence on J_{int}.

To evaluate the practical applicability of an OER catalyst, also the stability plays an important role and was investigated by applying a constant current density of 10 mA/cm^2 (Figure 4b). The potential obtained over Fe,Mn@DCD$_p$-600 °C increases directly and the catalyst deactivates within 1.3 h of reaction. Also the commercial NiCoO$_x$ shows a low stability as it deactivates within the first 2 h of reaction. With increasing pyrolysis temperature, an increasing stability of up to 22.6 h for Fe,Mn@DCD$_p$-800 °C is obtained. Further increase of the pyrolysis temperature to 900 °C or the treatment of the material with H_2SO_4 leads to a decreased stability of 4.7 h and 8.7 h, respectively. Compared to literature reported results for carbon-based materials, the prepared Fe,Mn@DCD$_p$-materials show lower or comparable OP and a higher stability (Table 2).[30,53] The stability of the prepared materials is even higher than obtained for IrO$_x$,[9] the OP is not as low.

The especially high stability of Fe,Mn@DCD$_p$-800 °C can be explained by taking a look at the STEM images, revealing that the complete surface of the MWCNT is covered with metal spinel particles protecting the surface of the MWCNT. As instability due to oxidation in corrosive electrolyte is a frequently reported issue of carbon-based materials in the OER, the spinel nanoparticles seem to be beneficial to protect the MWCNT from decomposition.[54] Thus, catalytic activity and stability of the materials are both highly influenced by the variation of the pyrolysis temperature. At temperatures above 800 °C, the formed Fe$_3$C inside the MWCNT decomposes to Fe^0 and graphitic carbon. The improved stability of the materials results from Mn$_3$O$_4$ and Fe$_3$O$_4$ spinel nanoparticles, covering the outer surface of the MWCNT and thereby protecting the catalyst from oxidation. The activity instead rather results from the N-rich MWCNT, the metal oxides incorporated in their structure, and the Fe$_3$C particles inside.

Table 2. Electrochemical surface area (*ECSA*), OP, intrinsic activity (J_{int}) and stability of Fe,Mn@DCD$_p$-materials and commercial NiCoO$_x$ compared to literature reported results.

Material Fe, Mn@DCDp-	ECSA [cm^2]	OP [mV]	J1.58 V [mA/cm^2]	Jint [mA/cm^2]	Stability [h]
600 °C[a]	0.26	549	0.07	0.038	1.29
700 °C[a]	0.38	405	2.34	0.869	11.4
800 °C[a]	13.2	389	2.39	0.025	22.6
900 °C[a]	1.12	463	0.28	0.035	4.70
800 °C-H_2SO_4[a]	2.23	397	2.22	0.138	8.68
NiCoO$_x$[a]	1.75	390	1.99	0.159	1.91
CMK-3-MnPc-WI[a],[53]	–	490	0.1	–	< 0.1
IrO$_x$[b],[9]	21	320	42	–	< 2
MnO$_x$/NCNT[c],[30]	–	520	< 0.5	–	> 5

Electrolyte: [a] 1 M KOH, [b] 1 M NaOH, [c] 0.1 M KOH.

Conclusion

In the presented study a series of carbon-based composite materials containing different Fe and Mn species were synthesized and extensively characterized by N$_2$-physisorption, CHN, ICP-OES, Raman spectroscopy, XPS, STEM(-EDX), and XRD. The complementary methods reveal that a minimum temperature of 700 °C is needed to ensure the formation of highly graphitic and conductive N-rich MWCNT. The materials are decorated on their outer surface with Mn$_3$O$_4$ and Fe$_3$O$_4$ spinel nanoparticles. Importantly, Fe and Mn oxides are also firmly incorporated into the carbon matrix. Furthermore, the tubes contain Fe$_3$C particles inside that decompose to Fe^0 particles and graphitic carbon at elevated pyrolysis temperatures. Electrochemical measurements of the composite materials revealed that the MWCNT with incorporated N-moieties and Fe and Mn oxides as well as the Fe$_3$C particles contribute to a high OER activity. The most active catalyst synthesized at a pyrolysis temperature of 800 °C achieves a low OP of 389 mV. Additionally, the spinel nanoparticles covering the outer surface of the electrocatalyst ensure a stability of up to 22.6 h, which is high for a carbon-based OER electrocatalyst and a step forward to practical application. The study shows that the adjustment of different material properties can lead to an optimized composite material, which enables the OER with simultaneously high activity and stability.

Experimental Section

Ethanol (99.8 %), Nafion® (5 wt.% in lower aliphatic alcohols containing 15–20 % water), NiCoO$_x$ and MnCl$_2$ were purchased from Sigma-Aldrich. FeCl$_2$ anhydrous (99.5 %), FeCl$_3$ anhydrous (98 %) and DCD (99 %) were obtained from Alfa Aesar. H$_2$SO$_4$ (38 %) was purchased from ChemSolute. N$_2$-Physisorption was performed on an Asap 2000 from Micromeritics. The samples were dried for 24 h at 300 °C under vacuum prior to measurement. The structure of the samples was observed and measured by STEM and STEM-EDX

(Hitachi HD-2700 Cs-corrected, 200 kV, Cold FEG, EDAX Octane T Ultra W 200 mm2 SDD TEAM-Software). The wall thickness of MWCNT was derived from STEM images using the software image J. XRD patterns were recorded with a Bruker D8 Advance instrument using Cu K_α radiation, grazing incident for the incoming beam and a Goebel mirror. Confocal Raman Microscopy images were obtained with a WITec Alpha 300R microscope, equipped with a 532 nm solid state laser. ICP-OES was performed on an ICP Spectroflame D by Spectro. A 2400 CHNS/O Series II System by PerkinElmer was used for elemental analysis. XPS analysis was performed using a Kratos Axis Ultra DLD device. Spectra were referenced to sp^2-hybridised carbon at 284.5 eV.

Synthesis of electrocatalysts

Fe,Mn@DCD_p-materials were synthesized by mixing DCD (0.60 g, 0.0072 mol) with $FeCl_2$ (0.22 g, 0.0017 mol), $FeCl_3$ (0.27 g, 0.0017 mol) and $MnCl_2$ (0.43 g, 0.0034 mol). All chemicals were milled until a homogeneous orange colored powder was obtained. The mixture was pyrolyzed at 600 °C to 900 °C in a tube furnace for 1 h under nitrogen atmosphere. A heating rate of 1 °C/min was used. The catalyst was ball milled until a fine brownish powder was obtained. The powder was ultra-sonicated in 1 M NaOH solution for 1 h, centrifuged at 6000 rpm for 15 minutes and decanted. The sediment was dispersed in distilled water and centrifugation was repeated five times to ensure a neutral pH of the supernatant solution. Finally, the catalyst was dried at 100 °C overnight.

To manufacture Fe,Mn@DCDp-800 °C-H_2SO_4, Fe,Mn@DCDp-800 °C was stirred in 1 M H_2SO_4 solution at room temperature (RT) for 24 h. The solution was centrifuged, decanted, washed neutral and dried at 100 °C in an oven overnight.

Electrochemical measurements

Catalyst inks were prepared by dispersing the catalyst (2.2 mg) in a mixture of milli Q water (49 μL), ethanol (49 μL) and Nafion (2 μL). The ink was ultra-sonicated for 15 min. 2.5 μL of catalyst ink was pipetted onto the glassy carbon rotating disk electrode (RDE) and dried at RT for 30 min. The tip possesses a geometric surface area of 0.1396 cm^2. Therefore, a catalyst film with a loading of 89.5 $\mu g_{catalyst}/cm^2$ resulted.

Electrochemical measurements were performed in a glass cell using a three electrode setup at RT. The modified glassy carbon RDE was used as working electrode. A glassy carbon and an Ag/AgCl (3 M KCl) electrode were used as the counter and the reference electrode, respectively. 1 M KOH was used as electrolyte. The electrocatalytic activity was investigated by LSV using an Autolab potentiostat by Metrohm. Potentials were referenced to the reversible hydrogen electrode (RHE). Before data aquisition, the catalysts underwent continuous potential cycling (CV) until steady voltammograms were obtained (100 CVs @ 0.1 V/s). Afterwards LSV was carried out in a potential range of 1.00 to 1.86 V at a rotation speed of the working electrode of 1600 rpm and a scan rate of 5 mV/s. c_{DL} was measured by CV scans at various scan rates in the range 1.0 to 1.1 V *vs.* RHE. EIS was performed at an OP of 179 mV with an amplitude of the sinusoidal voltage perturbation of 10 mV over a frequency range of 100 kHz to 50 mHz. The long-term performance was investigated by applying a steady current density of 10 mA/cm^2.

Acknowledgements

The authors acknowledge the Federal Ministry of Education and Research (BMBF) for funding this work within the MANGAN research cluster (FKZ 03SF0508). Feng Zeng acknowledges the China Scholarship Council for financial support. We thank the laboratory technicians Jens Heller and Christine Bollig for experimental support.

Open access funding enabled and organized by Projekt DEAL.

Conflict of Interest

The authors declare no conflict of interest.

[1] J. A. Turner, *Science* **2004**, *305*, 972–974.
[2] M. G. Schultz, T. Diehl, G. P. Brasseur, W. Zittel, *Science* **2003**, *302*, 624–627.
[3] S. Chu, A. Majumdar, *Nature* **2012**, *488*, 294.
[4] D. L. Stojić, M. P. Marčeta, S. P. Sovilj, Š. S. Miljanić, *J. Power Sources* **2003**, *118*, 315–319.
[5] G. W. Crabtree, M. S. Dresselhaus, M. V. Buchanan, *Phys. Today* **2004**, *57*, 39–44.
[6] P. P. Edwards, V. L. Kuznetsov, W. I. F. David, N. P. Brandon, *Energy Policy* **2008**, *36*, 4356–4362.
[7] J. Suntivich, K. J. May, H. A. Gasteiger, J. B. Goodenough, Y. Shao-Horn, *Science* **2011**, *334*, 1383–1385.
[8] T. Reier, M. Oezaslan, P. Strasser, *ACS Catal.* **2012**, *2*, 1765–1772.
[9] C. C. L. McCrory, S. Jung, J. C. Peters, T. F. Jaramillo, *J. Am. Chem. Soc.* **2013**, *135*, 16977–16987.
[10] J. Rossmeisl, Z. W. Qu, H. Zhu, G. J. Kroes, J. K. Nørskov, *J. Electroanal. Chem.* **2007**, *607*, 83–89.
[11] Y. Lee, J. Suntivich, K. J. May, E. E. Perry, Y. Shao-Horn, *J. Phys. Chem. Lett.* **2012**, *3*, 399–404.
[12] K. A. Stoerzinger, L. Qiao, M. D. Biegalski, Y. Shao-Horn, *J. Phys. Chem. Lett.* **2014**, *5*, 1636–1641.
[13] H. Wang, Q. Gao, L. Jiang, *Small* **2011**, *7*, 2454–2459.
[14] H. Wang, X. Wang, *ACS Appl. Mater. Interfaces* **2013**, *5*, 6255–6260.
[15] F. Zeng, C. Broicher, J. P. Hofmann, S. Palkovits, R. Palkovits, *ChemCatChem* **2020**, *12*, 710–716.
[16] R. Gao, D. Yan, *Adv. Energy Mater.* **2020**, *10*, 1900954.
[17] C. Leal-Rodríguez, D. Rodríguez-Padrón, Z. A. Alothman, M. Cano, J. J. Giner-Casares, M. J. Muñoz-Batista, S. M. Osman, R. Luque, *Nanoscale* **2020**, *12*, 8477–8484.
[18] Y. Cheng, S. P. Jiang, *Pro. Nat. Sci.-Mater.* **2015**, *25*, 545–553.
[19] T. Y. Ma, S. Dai, S. Z. Qiao, *Mater. Today* **2016**, *19*, 265–273.
[20] M. S. Ahmed, B. Choi, Y.-B. Kim, *Sci. Rep.* **2018**, *8*, 2543.
[21] A. K. Beine, C. Broicher, Q. Hu, L. Mayerl, T. Bisswanger, H. Hartmann, A. Besmehn, S. Palkovits, A.-H. Lu, R. Palkovits, *Catal. Sci. Technol.* **2018**, *8*, 6311–6315.
[22] H. Xu, J. Wu, W. Luo, Q. Li, W. Zhang, J. Yang, *Small* **2020**, 2001775.
[23] M. Gong, Y. Li, H. Wang, Y. Liang, J. Z. Wu, J. Zhou, J. Wang, T. Regier, F. Wei, H. Dai, *J. Am. Chem. Soc.* **2013**, *135*, 8452–8455.
[24] R. Arrigo, S. Wrabetz, M. E. Schuster, D. Wang, A. Villa, D. Rosenthal, F. Girsgdies, G. Weinberg, L. Prati, R. Schlögl, D. S. Su, *Phys. Chem. Chem. Phys.* **2012**, *14*, 10523–10532.
[25] P. Chen, L. M. Chew, A. Kostka, M. Muhler, W. Xia, *Catal. Sci. Technol.* **2013**, *3*, 1964–1971.
[26] W.-J. Jiang, L. Gu, L. Li, Y. Zhang, X. Zhang, L.-J. Zhang, J.-Q. Wang, J.-S. Hu, Z. Wei, L.-J. Wan, *J. Am. Chem. Soc.* **2016**, *138*, 3570–3578.
[27] M. Tavakkoli, T. Kallio, O. Reynaud, A. G. Nasibulin, J. Sainio, H. Jiang, E. I. Kauppinen, K. Laasonen, *J. Mater. Chem. A* **2016**, *4*, 5216–5222.
[28] Y. Xu, Y. Yan, T. He, K. Zhan, J. Yang, B. Zhao, K. Qi, B. Y. Xia, *Carbon* **2019**, *145*, 201–208.
[29] L. Su, D. Han, G. Zhu, H. Xu, W. Luo, L. Wang, W. Jiang, A. Dong, J. Yang, *Nano Lett.* **2019**, *19*, 5423–5430.
[30] H. Antoni, W. Xia, J. Masa, W. Schuhmann, M. Muhler, *Phys. Chem. Chem. Phys.* **2017**, *19*, 18434–18442.

[31] J. Masa, W. Xia, I. Sinev, A. Zhao, Z. Sun, S. Grützke, P. Weide, M. Muhler, W. Schuhmann, *Angew. Chem. Int. Ed.* **2014**, *53*, 8508–8512; *Angew. Chem.* **2014**, *126*, 8648–8652.
[32] Z. Wen, S. Ci, Y. Hou, J. Chen, *Angew. Chem. Int. Ed.* **2014**, *53*, 6496–6500; *Angew. Chem.* **2014**, *126*, 6614–6618.
[33] X. Ma, H. Chai, Y. Cao, J. Xu, Y. Wang, H. Dong, D. Jia, W. Zhou, *J. Colloid Interface Sci.* **2018**, *514*, 656–663.
[34] J.-S. Li, S.-L. Li, Y.-J. Tang, M. Han, Z.-H. Dai, J.-C. Bao, Y.-Q. Lan, *Chem. Commun.* **2015**, *51*, 2710–2713.
[35] Y. Zhang, J. Zai, K. He, X. Qian, *Chem. Commun.* **2018**, *54*, 3158–3161.
[36] Y. Lan, J. Chen, H. Zhang, W.-x. Zhang, J. Yang, *J. Mater. Chem. A* **2020**, doi: 10.1039/D0TA02317E.
[37] B. K. Barman, K. K. Nanda, *Green Chem.* **2016**, *18*, 427–432.
[38] B. Wang, Y. Hu, B. Yu, X. Zhang, D. Yang, Y. Chen, *J. Power Sources* **2019**, *433*, 126688.
[39] W. Li, Y. Chen, B. Yu, Y. Hu, X. Wang, D. Yang, *Nanoscale* **2019**, *11*, 17031–17040.
[40] C. Huang, B. Zhang, Y. Luo, D. Xiao, K. Tang, Q. Ruan, Y. Yang, B. Gao, P. K. Chu, *Appl. Surf. Sci.* **2020**, *507*, 145155.
[41] Y. Wang, G. Zhang, G. Liu, W. Liu, H. Chen, J. Yang, *RSC Adv.* **2016**, *6*, 44013–44018.
[42] L. Wang, Y. Li, Z. Han, L. Chen, B. Qian, X. Jiang, J. Pinto, G. Yang, *J. Mater. Chem. A* **2013**, *1*, 8385–8397.
[43] K. Song, Y. Lee, M. R. Jo, K. M. Nam, Y.-M. Kang, *Nanotechnology* **2012**, *23*, 505401.
[44] J. F. Moulder, W. F. Stickle, P. E. Sobol, K. D. Bomben in *Handbook of X-ray Photoelectron Spectroscopy* (Ed. Jill Chastain), Perkin-Elmer Corporation, Eden Prairie, **1992**, pp. 78–79.
[45] T. Yamashita, P. Hayes, *Appl. Surf. Sci.* **2008**, *254*, 2441–2449.
[46] M. C. Biesinger, B. P. Payne, A. P. Grosvenor, L. W. M. Lau, A. R. Gerson, R. S. C. Smart, *Appl. Surf. Sci.* **2011**, *257*, 2717–2730.
[47] X. Zhao, Y. Ando, *Jpn. J. Appl. Phys.* **1998**, *37*, 4846–4849.
[48] G. Jian, Y. Xu, L.-C. Lai, C. Wang, M. R. Zachariah, *J. Mater. Chem. A* **2014**, *2*, 4627–4632.
[49] Y. Zhao, J. Zhang, X. Guo, H. Fan, W. Wu, H. Liu, G. Wang, *J. Mater. Chem. A* **2017**, *5*, 19672–19679.
[50] G. Brooks, F. Huo in *Electric Furnace Conference Proceedings*, *Vol. 57*, **1999**, pp. 731–740.
[51] K. H. Cho, H. Seo, S. Park, Y. H. Lee, M. Y. Lee, N. H. Cho, K. T. Nam, *Adv. Funct. Mater.* **2020**, *30*, 1910424.
[52] M. Wei, Y. Han, Y. Liu, B. Su, H. Yang, Z. Lei, *J. Alloys Compd.* **2020**, *831*, 154702.
[53] C. Broicher, J. Artz, S. Palkovits, H. Antoni, M. Drogeler, D. M. Morales, C. Stampfer, R. Palkovits, *Catal. Sci. Technol.* **2018**, *8*, 1517–1521.
[54] Y. Liu, J. Li, F. Li, W. Li, H. Yang, X. Zhang, Y. Liu, J. Ma, *J. Mater. Chem. A* **2016**, *4*, 4472–4478.

Manuscript received: June 5, 2020
Revised manuscript received: July 11, 2020
Accepted manuscript online: July 27, 2020
Version of record online: September 24, 2020